

An Evaluation of the Anti-diabetic Potential of *Rubia manjith* Roxburgh ex Fleming Using *In Vitro* and *In Silico* Methods

Sabin Khanal ¹, Prabhat Neupane ², Manila Poudel ³, Sujan Dhital ², Bindira Gosain ¹, Kanchan Shakhakarmi ¹, Samjhana Bharati ², Binita Maharjan ², Timila Shrestha ², Jhashanath Adhikari Subin ^{4,*}, Ram Lal Swagat Shrestha ^{2,*}, Bishnu P. Marasini ^{1,3,5,*}

¹ Department of Pharmacy, National Model College for Advance Learning, National College, Tribhuvan University, Lainchaur, Kathmandu 44600, Nepal; khanalsabin09@gmail.com (S.K.); bindiragosain@gmail.com (B.G.); kshakhakarmi@gmail.com (K.S.); bishnu.marasini@gmail.com (B.P.M.);

² Department of Chemistry, Amrit Campus, Tribhuvan University, Lainchour, Kathmandu 44600, Nepal; neupaneprabhat1998@gmail.com (P.N.); sujandhital07@gmail.com (S.D.); bharati.samjhana@gmail.com (S.B.); binitamhrjan@gmail.com (B.M.); timilastha@gmail.com (T.S.); swagatstha@gmail.com (R.L.S.S.);

³ Department of Biotechnology, National College, Tribhuvan University, Lainchour, Kathmandu 44600, Nepal; paudelmanila@gmail.com (M.P.);

⁴ Bioinformatics and Cheminformatics Division, Scientific Research and Training Nepal P. Ltd., Kaushaltar, Bhaktapur 44800, Nepal; subinadhikari2018@gmail.com (J.A.S.);

⁵ Nepal Health Research Council, Ministry of Health and Population, Ramshah Path, Kathmandu 44600, Nepal

* Correspondence: subinadhikari2018@gmail.com (J.A.S.); swagatstha@gmail.com (R.L.S.S.); bishnu.marasini@gmail.com (B.P.M.);

Received: 29.08.2024; Accepted: 11.04.2025; Published: 22.07.2025

Abstract: This study, combining biological assays of *Rubia manjith* Roxburgh ex Fleming with computational analysis, aims to identify potential α -glucosidase and α -amylase inhibitors from a pool of compounds sourced through a literature survey. The potential inhibitory activities of *Rubia manjith* were investigated using experimental and computational approaches. The chloroform extract of the plant showed significant antioxidant activity (87.4%) with an IC_{50} of 53.1 ± 0.5 μ g/mL. It notably inhibited α -amylase (75.8%, $IC_{50} = 113.9 \pm 3.6$ μ g/mL) and α -glucosidase (72.9%, $IC_{50} = 32.9 \pm 0.4$ μ g/mL). Selected phytochemicals were docked against the enzymes, followed by molecular dynamics simulations. Compound 1 had docking scores of -10.0 and -9.2 kcal/mol against α -glucosidase and α -amylase, respectively, with native ligand scores of -8.6 and -8.0 kcal/mol. RMSD profiles suggested good geometrical stability, and binding free energy changes of -24.70 ± 7.94 and -14.47 ± 6.19 kcal/mol for α -glucosidase and α -amylase complexes, respectively, hinted at sustained spontaneity of complex formation. Compound 2 also showed good geometrical and thermodynamic parameters against α -glucosidase. These findings offer valuable insights for subsequent *in vitro* testing of the hit compounds in the diabetes drug development process. Further validation, including drug-likeness and safety assessments, could be broadened through additional *in silico*, *in vitro*, and *in vivo* trials.

Keywords: α -amylase; α -glucosidase; molecular docking; molecular dynamics simulation.

© 2025 by the authors. This article is an open-access article distributed under the terms and conditions of the Creative Commons Attribution (CC BY) license (<https://creativecommons.org/licenses/by/4.0/>), which permits unrestricted use, distribution, and reproduction in any medium, provided the original work is properly cited. The authors retain copyright of their work, and no permission is required from the authors or the publisher to reuse or distribute this article, as long as proper attribution is given to the original source.

1. Introduction

Herbal medicine has a long history in the treatment of various diseases and is in use because of some inherent active ingredients [1-3]. The World Health Organization (WHO) suggests that medicinal plants represent an optimal resource for acquiring a diverse range of pharmaceuticals [4]. Hence, it is imperative to conduct thorough research on these plants to comprehend their characteristics, safety profiles, and effectiveness.

Rubia manjith is a climbing perennial herb distributed in Nepal, India, and China at an altitude of about 1200 to 3200 m [5]. Traditionally, root powder of the plants is used as an antiseptic, antidiarrheal, and antihelminthic tonic. Additionally, the root is used to treat leprosy, rheumatoid arthritis, neuralgia, diarrhea, skin conditions, wounds, pharyngitis, coughs, diabetes, and delayed healing of fractured bones. Moreover, *R. manjith* has also been linked with ayurvedic medicine for diabetes management [6]. Lately, there has been a synergistic approach in the drug development process toward computational methods, primarily driven by their efficiency and cost-effectiveness [7,8]. This investigation integrates molecular docking, molecular dynamics simulation (MDS), and binding free energy calculations to pinpoint the optimally docked ligand with the greatest stability, demonstrating its potential for inhibiting the receptor protein.

Diabetes is a chronic condition that occurs when the body cannot produce enough insulin or cannot use it effectively, and it is diagnosed by observing elevated levels of glucose in the blood [9,10]. The WHO estimates that currently, more than 180 million people worldwide have diabetes, with India, China, and the United States predicted to have the largest number of affected individuals. As per the estimations provided by the International Diabetes Federation, the prevalence of diabetes, standing at 10.5% in 2021, is expected to climb to 11.3% by 2030 and to 12.2% by 2040 [11]. Pancreatic α -amylase and α -glucosidase are some of the important digestive enzymes. The pancreatic α -amylase acts as a catalyst in the reaction that involves the hydrolysis of the α -1,4 glycosidic linkages in starch, amylopectin, amylose, glycogen, and numerous maltodextrins, being responsible for starch digestion. The enzyme α -glucosidase hydrolyzes disaccharides and oligosaccharides, which can form absorbable glucose. Inhibitors of these enzymes can retard the liberation of glucose from carbohydrates, resulting in reduced postprandial plasma glucose levels and the suppression of postprandial hyperglycemia [12]. Therefore, one strategy for maintaining and lowering blood glucose levels is by delaying glucose absorption through the inhibition of α -amylase and α -glucosidase along the digestive tract. This lab-based study, followed by a computational study, aims to identify potential α -glucosidase and α -amylase inhibitors from a pool of compounds prepared from a literature survey, reported to be isolated from *R. manjith* as done in a study by Kumar and team [13]. Bridging traditional practices with modern scientific understanding is crucial for designing effective and safer drug-like molecules in the pursuit of therapeutic solutions.

2. Materials and Methods

2.1. Plant collection.

The plant part was collected from Arghakhanchi, Nepal, which was duly identified as *Rubia manjith* Roxburgh ex Fleming (voucher code: NCB170) at the National Herbarium and Plant Research, Lalitpur, Nepal.

2.2. Preparation of extracts.

Powder (50 gm) form of the root of *R. manjith* was extracted for 8 hours using water, hexane, chloroform, and ethanol (250 mL) with respect to increasing polarity in the Soxhlet apparatus. The extract was then evaporated to dryness, and the percentage yield was calculated. The final dry crude extract was stored in a cold place until it was used for the experiments.

$$\text{PercentageYield}(\%) = \frac{\text{Dryweightofextract}}{\text{Totalweightofpowder}} \times 100 \quad (1)$$

2.3. Determination of total phenol content.

The total phenol content of the extracts was measured using the Folin-Ciocalteu method [14]. The reaction was done in a 200 μL final volume by adding 20 μL of plant extracts. In each well, 100 μL of Folin-Ciocalteu and 80 μL of Na_2CO_3 were added to standards and samples. After incubating in the dark for 30 minutes, absorbance was measured at 765 nm with a UV spectrophotometer (Epoch, BioTek, USA).

2.4. Determination of total flavonoid content.

The reaction was conducted in a 200 μL final volume by combining 20 μL of a 500 $\mu\text{g}/\text{mL}$ plant extract with 110 μL of distilled water in each well-containing plant sample, maintaining a final volume of 130 μL . Subsequently, 60 μL of ethanol, 5 μL of AlCl_3 , and 5 μL of potassium acetate were added to each well containing standard and plant sample. The mixture was left in the dark for 30 minutes, and absorbance was measured at 415 nm using a UV spectrophotometer [15].

2.5. DPPH free radical scavenging assay.

Equal volumes of DPPH were added to the sample in a 1:1 ratio at various concentrations. The mixture was incubated in the dark for 15 minutes, after which the absorbance was taken at 517 nm [16,17]. The ability to scavenge the DPPH radical was determined by the reduction of absorbance and calculated using the following equation:

$$\% \text{scavanging} = \frac{A_0 - A_t}{A_0} \times 100 \quad (2)$$

Where A_0 is the absorbance of DPPH with 3% DMSO and A_t is the absorbance of DPPH with test or reference sample

2.6. Alpha-amylase inhibition assay.

The α -amylase inhibition activity was assessed using 50 mM phosphate buffer at pH 6.8. Initially, 80 μL of amylase at a final concentration of 1.5 units/mL was added to each well. Subsequently, various concentrations of 20 μL test compounds (prepared in DMSO) were incubated at 37°C for 15 minutes, and the initial absorbance was recorded. The reaction was initiated by adding 100 μL of the substrate 2-chloro-4-nitrophenyl- α -D maltotrioside (CNP G_3) (375 μM) immediately after incubation, prepared in the aforementioned buffer to maintain a final volume of 200 μL [18].

$$\% \text{inhibition} = \frac{A_0 - A_t}{A_0} \times 100 \quad (3)$$

Where A_0 is the absorbance of enzyme-substrate reaction with 5% DMSO, and A_t is the absorbance of enzyme-substrate with plant extract.

2.7. Alpha-glucosidase inhibition assay.

α -glucosidase (0.2 Units) was premixed with 5 $\mu\text{g/mL}$ of the extract in 50 mM phosphate-buffered saline (PBS) at pH 6.8, and the final concentration was maintained up to 100 $\mu\text{g/mL}$. Subsequently, 0.7 mM 4-nitrophenyl β -D glucopyranoside (PNPG) was added. This reaction mixture was incubated in a 96-well plate reader at 37°C for 15 minutes, and OD was recorded at 410 nm [19].

The percentage α -glucosidase inhibitory effect was calculated by the following formula:

$$\% \text{inhibition} = \frac{A_0 - A_t}{A_0} \times 100 \quad (4)$$

Where A_0 is the absorbance of enzyme-substrate reaction with 50% DMSO and A_t is the absorbance of enzyme-substrate reaction from the plant extract.

2.8. Computational procedures.

2.8.1. Selection and preparation of ligands database.

A database of fifteen ligands was prepared through a literature review of isolated compounds from *Rubia manjith* [20-25], as shown in (Figure S1). 2D structures of ligands were sketched, converted, and saved in 3D PDB format [26]. Energy minimization was carried out using the Avogadro program with the conjugate gradient approach. The energy convergence was set at 10^{-8} units, and a universal force field (UFF) for 5000 cycles was taken [27]. The molecular structure was optimized until there were no noticeable changes in atomic positions and energy reduction. Rotatable bonds for each ligand were identified, and non-polar hydrogens were merged. Subsequently, using the AutoDock Tools [28], the structure was converted into PDBQT format by adding Gasteiger charges.

2.8.2. Target selection and preparation.

From the RCSB database, the crystal protein structure of α -glucosidase (PDB ID: 5ZCC) with a resolution of 1.70 Å (X-ray diffraction) and α -amylase (PDB ID: 4GQR) with a resolution of 1.20 Å (X-ray diffraction) was retrieved [29]. Since there were missing amino acid residues in the α -glucosidase structure, homology modeling was performed using the Swiss Modeling server [30]. The protein was cleaned using the PyMOL software [31], which involved the removal of co-crystallized ligands, water molecules, ions, and co-factors. Subsequently, polar hydrogens and Kollman charges were added through the AutoDock Tools and were converted to PDBQT format, as required for molecular docking.

2.8.3. Molecular docking calculations.

The binding poses and comparative binding affinities between the ligand and the receptor were calculated from molecular docking studies using AutoDock Vina software. Control parameters such as the number of modes of 20, the energy range of 4 units, and the exhaustiveness of 64 were selected for the docking process. For α -glucosidase, grid center of (-0.655, 53.715, and 72.724) and a box size of $30 \times 30 \times 30 \text{ \AA}^3$ with 0.375 Å spacing were selected. Similarly, grid center of (16.731, 17.235, 42.467) and box size of $44 \times 46 \times 44 \text{ \AA}^3$ with 0.375 Å spacing were employed in the case of α -amylase. Through molecular docking calculations, the ideal protein-ligand complex with the highest binding affinity (kcal/mol) was

identified. The scoring function comprises six components: $E_{\text{Rotational}}$, E_{Gauss1} , $E_{\text{Hydrogen Bond}}$, E_{Gauss2} , $E_{\text{Repulsion}}$, and $E_{\text{Hydrophobic}}$. Among these, rotation and repulsion are the two destabilizing energy components, whereas the other four represent stabilizing energy. The molecular docking protocol validation was done through the superimposition of docked native ligand with ligand in the holo-structure of protein. A good RMSD value of 0.5 Å was obtained for α -glucosidase, and an acceptable RMSD value of 2.5 Å was observed in the case of α -amylase [32-34]. The Biovia Discovery Studio program was used for 2D and 3D visualization of protein-ligand interactions [35]. The pose with the best binding energy was chosen for analysis, additional investigation, and molecular dynamics simulation.

2.8.4. Molecular dynamics simulation (MDS).

The MDS of the ligand-protein complexes was performed using the GROMACS program [36], and the Charmm27 force field [37] from the SwissParam server [38] was used for both the ligand and the receptor. Utilizing the TIP3P water model, a triclinic box system with the adduct was solvated. To minimize the spurious interactions between the periodic images, 12 Å spacing at the sides was employed. The system was neutralized, and an isotonic solution of NaCl (0.15 M) was used. It was then equilibrated in four stages, i.e., two NVT equilibriums (500 ps and 600 ps) and the final two NPT equilibriums (500 ps and again 500 ps) each at a physiological temperature of 310 K. The final production run was conducted for 200 ns without any restrains, and utilizing built-in modules, several parameters, including SASA, R_g , RMSD, and RMSF, were extracted from the MDS trajectory. The protein-ligand complex's stability during the production run was evaluated using these geometrical parameters. All other parameters used by Sharma et al. and Neupane et al. were adopted [39,40].

2.8.5. Binding free energy change estimation.

The changes in binding free energy of the complex were determined using the Poisson-Boltzmann solvation model as implemented in the MMPBSA method [41]. The spontaneity and feasibility of the forward reaction were assessed based on end-state binding free energy changes. For its calculation, an equilibrated portion of the trajectory (200 frames) was employed with the `gmx_MMPBSA` tool of the GROMACS program in the conda environment.

The changes in binding free energy of the protein-ligand complex are given by linear equation (1) [42].

$$\Delta G_{\text{BFE}} = \Delta G_{\text{complex}} - \Delta G_{\text{protein}} - \Delta G_{\text{ligand}} \quad (1)$$

$$\Delta G_{\text{BFE}} = \Delta G_{\text{GAS}} + \Delta G_{\text{Solvent}} \quad (2)$$

And can be decomposed as equation (3)

$$\Delta G_{\text{BFE}} = \Delta G_{\text{VDW}} + \Delta G_{\text{EL}} + \Delta G_{\text{PB}} + \Delta G_{\text{SURF}} \quad (3)$$

Equation (2)'s right-hand side has two components that represent gas phase energies (ΔG_{GAS}) and solvation ($\Delta G_{\text{Solvent}}$), respectively.

2.9. Statistical analysis.

The results of the spectrophotometric analyses, such as enzyme assays, were processed using Gen5 Microplate. The collected data were analyzed with Microsoft Excel (2016) was also employed for additional analysis. The IC_{50} (Inhibition of enzymatic hydrolysis of the substrate by 50%) was calculated using the EZ-Fit software (Perellela Scientific, Inc., Amherst,

Mars, USA). The results were presented as the mean \pm standard error from triplicate experiments.

3. Results and Discussion

3.1. Percentage yield and phytochemical screening.

The highest yield of the *R. manjith* was achieved with the ethanolic extract (13.1%), followed by the chloroform extract (1.2%), and the lowest in the hexane extract (0.93%), as shown in (Table S1). A study conducted by Chandrashekhar et al. found a percentage yield of 11.63 % in chloroform extract [43]. Phytochemical screening showed the presence of different phytochemical compounds, such as alkaloids, steroids, tannin, saponin, polyphenols, terpenoids, and glycosides, as shown in (Table S2). The majority of antioxidant action is attributed to phenolic chemicals that contain free hydrogen. Flavonoids, tannins, polyphenols, and reducing sugar all contribute significantly to antioxidant activity. *Rubia* contains a wide variety of antioxidants, such as alizarin, hydroxyl anthraquinones, and rubiadin, which have been used in various medicaments [44,45].

3.2. DPPH (α , α -diphenyl- β -picrylhydrazyl) free radical scavenging assay.

The chloroform extract of *R. manjith* exhibited the highest free radical scavenging activity at 87.4% with an IC₅₀ of 53.1 \pm 0.5 μ g/mL, as observed in (Table S3). Our results align with those reported by Deoda's study, where the chloroform extract of *Rubia* demonstrated potent protective action [46]. This activity might be influenced by climatic variation, geographical differences, or the solvent used for extraction, as well as the high-grade chemicals or the authenticity of the sample.

3.3. Total phenolic and flavonoid content.

The hexane extract of *R. manjith* showed the highest concentration of TPC at 2.65 \pm 0.01 mg GAE/gm, while the lowest concentration was observed in the ethanol extract (0.10 \pm 0.01 mg GAE/gm), as shown in (Table S4). In the TFC test, ethanolic extract of *R. manjith* was found to have the highest (0.34 \pm 0.01 mg QE/gm) TFC, whereas hexane extract was found to have the lowest TFC (0.03 \pm 0.01 mg QE/gm) as demonstrated in (Table S5).

In a study by Srabana and Kshitij in 2017, the determination of TPC and TFC yielded values of (41.1 \pm 0.8 mg GAE/gm) and (30.1 \pm 1.3 mg QE/gm), respectively [47]. These values differ from the results of our study. This discrepancy might be attributed to geographical variation, plant variability, time of study, UV light, pathogenic attack, and pollution, according to a paper by Manach and group [48].

3.4. Alpha-amylase inhibition assay.

The α -amylase inhibition potential of plant extracts was analyzed based on their IC₅₀ values, representing the concentrations causing 50% inhibition. The chloroform extract sample exhibited the highest α -amylase inhibition at 75.8%, with an IC₅₀ value of 113.9 \pm 3.6 μ g/mL, suggesting strong potency in inhibiting the α -amylase's activity. In contrast, the ethanol extract showed 17% inhibition, while the hexane extract exhibited the lowest inhibition at 6.9%, as displayed in (Table S6). Ethanol, chloroform, and hexane plant extracts are found to be α -amylase digestive enzyme inhibitors, as mentioned by Kunwar [49]. While the IC₅₀ value of

the positive control, acarbose, is lower at 6.1 $\mu\text{g/mL}$ compared to the plant extracts, it is expected that the extracts would have higher IC_{50} values. This is because plant extracts consist of a multitude of compounds, unlike the single compound acarbose, as described by Khadayat [18].

3.5. *Alpha-glucosidase inhibition assay.*

The α -glucosidase inhibition potential of different plant extracts was evaluated at 500 $\mu\text{g/mL}$. Acarbose was used as a standard reference (IC_{50} value $387.4 \pm 0.1 \mu\text{g/mL}$). The highest α -glucosidase inhibition was exhibited by chloroform extract of *R. manjith* (72.9%) with an IC_{50} value of $32.9 \pm 0.5 \mu\text{g/mL}$, as presented in (Table S7). Our findings align with the study by Kang [50], where the chloroform extract demonstrated significant inhibitory activity against α -glucosidase. The IC_{50} values for our three extracts, chloroform, hexane, and ethanol, were all lower than the IC_{50} value observed for acarbose ($387.36 \pm 0.05 \mu\text{g/mL}$).

3.6. *Docking scores and poses of ligands.*

Proteins can bind ligands at their orthosteric pocket based on the ligand's size, structure, functional groups, and other interactions [51-53]. Molecular docking calculations comprises of flexible ligand molecules docked into the pockets of rigid protein receptors. Structural optimization of ligands prior to molecular docking aims to reduce forces acting on each atom and minimize the ligand's total energy. By releasing strains from the ligand molecule, this optimization procedure provides the structure with its most stable form [54]. Based on the scoring components, molecular docking computations identify the optimal ligand positions and poses and provide numerical values as binding affinities, as shown in (Table S8). Docking the selected ligand database against the α -glucosidase protein revealed that most of the ligands possessed better binding affinity (kcal/mol) than that of the native ligand, which had -8.6 kcal/mol. The best binding affinity was observed with compound 1 having -10.0 kcal/mol. Similarly, compounds 2, 3, and 4 also demonstrated exemplary binding affinities, exceeding -9.0 kcal/mol. Moreover, compound 5 exhibited a good binding affinity of -8.9 kcal/mol.

Molecular docking against α -amylase protein revealed that compound 3 exhibited the highest binding affinity of -9.7 kcal/mol, surpassing that of the native ligand with -8.0 kcal/mol. Similarly, the binding affinities of -9.1 kcal/mol, -8.6 kcal/mol, -8.2 kcal/mol, and -8.0 kcal/mol were observed with compounds 1, 5, 7, and 11, respectively. Interestingly, the top candidates for α -glucosidase exhibited similar trends to those with α -amylase, suggesting that certain ligands (such as 1, 3, and 5) were capable of inhibiting both receptor molecules simultaneously. The better binding of these ligands compared to the native ligand indicated the presence of stronger interactions at the catalytic site of the protein. A higher negative value of binding affinity suggested a more favorable binding interaction between the receptor and ligand, suggesting their potential for diabetes management [55].

3.7. *Ligand-protein interactions in α -glucosidase complex.*

Several interactions, such as hydrogen bonds, carbon-hydrogen bonds, Pi-donor hydrogen bonds, Pi-anion, Pi-sigma, Pi-alkyl, Pi-Pi T-shaped, and van der Waals forces, were observed between the ligand and the active site residues of the α -glucosidase, as presented in (Table 1). In the case of the compound 1- α -glucosidase complex, a hydrogen bond was observed at a relatively shorter distance (2.45 Å), with amino acid residue ASP282 likely

playing a significant role in binding interactions. Additionally, a carbon-hydrogen bond and a Pi-donor hydrogen bond were observed with amino acid residues GLY384 and GLU141, respectively. Relatively weaker Pi-anion and Pi-alkyl interactions were formed between the ligand and amino acid residues ASP327, ALA200, PHE225, and ILE143. Multiple van der Waals interactions were also observed between the ligand and the receptor molecule that may provide significant support for binding, as depicted in (Figure 1) and will be dealt with in subsection 3.9.5 separately. In the case of the compound 2- α -glucosidase complex, multiple hydrogen bonds were observed at relatively shorter distances (2.09, 2.33, 2.90, and 2.92 Å) with amino acid residues SER145, ILE143, ASN258, and TRP288, respectively. Similarly, a carbon-hydrogen bond was observed with the PRO233 residue. Several hydrophobic interactions were observed with the amino acid residues GLU141, ILE143, PHE225, PRO233, and PHE282, as illustrated in (Figure 2). Moreover, various van der Waals interactions contributed to the overall binding between the ligand and the protein, as in the previous case.

Table 1. Binding affinities of top two protein-ligand complexes and their respective interactions with α -glucosidase

Ligands	Binding affinity (kcal/mol)	Types of interactions	Active site residues (Distance Å)
1	-10.0	Hydrogen bond	ASP382 (2.45)
		Carbon-hydrogen bond	GLN256 (3.13), GLY384 (3.62)
		Pi-donor hydrogen bond	GLU141 (3.43)
		Pi-anion	ASP327 (4.39, 4.95)
		Pi-alkyl	ILE143 (5.01, 4.55), ALA200 (4.76), PHE225 (5.03)
		van der Waals	ASP60, TYR63, SER142, PHE144, PHE163, ASP199, HIS203, GLN256, ASN258, PHE282, TRP288, MET385, TRY388, THR409, ARG411
2	-9.7	Hydrogen bond	ILE143 (2.90), SER145 (2.33), ASN258 (2.92), TRP288 (2.09)
		Carbon-hydrogen bond	PRO233 (3.10)
		Pi-sigma	PHE225 (3.80)
		Pi-anion	GLU141 (3.40)
		Pi-alkyl	PRO223 (4.66)
		Pi-Pi T-stacked	PHE282 (5.25)
		Alkyl	ILE143 (3.86, 4.90)
		van der Waals	SER142, PHE144, PHE163, SER224, GLY286, ASP327, GLN328, GLY384, MET385, TRY388, THR409, GLY410, ARG411

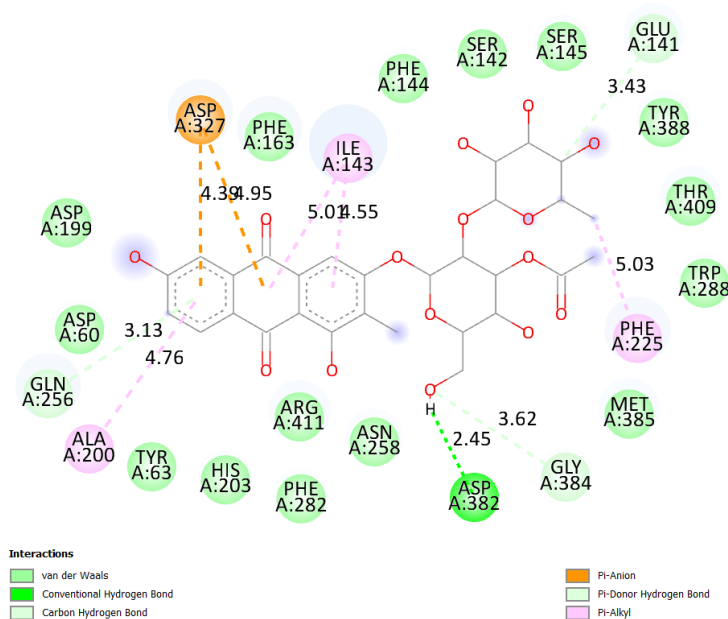


Figure 1. 2D representation of the interactions of compound 1 with α -glucosidase at the active pocket.

(3.74 Å) was observed with the amino acid residue HIS305. Furthermore, TRP59 formed a Pi-Pi stacked interaction with the ligand molecule, while an alkyl interaction was observed with LEU165 amino acid residue. Various amino acid residues were involved in van der Waals interactions with the ligand. Collectively, these interactions played a crucial role in the robust binding of the ligand to the active site of the receptor molecule, resulting in higher binding scores and are supported by thermodynamic parameters discussed later in the subsection.

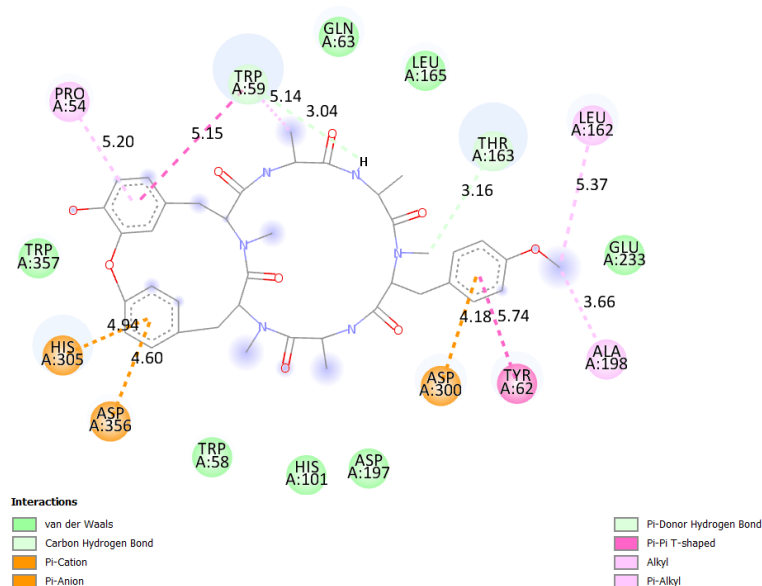


Figure 3. 2D representation of the interactions of compound 3 with α -amylase.

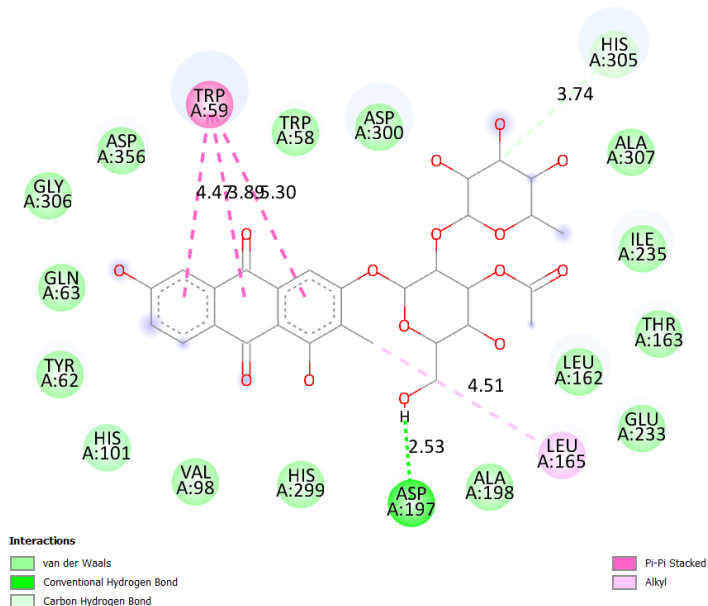


Figure 4. 2D representation of the interactions of compound 1 with α -amylase.

3.9. Geometrical descriptions from MDS.

3.9.1. Root mean square deviation (RMSD).

The RMSD curves of the ligand and protein backbone were extracted separately, both relative to the protein backbone from 200 ns MDS trajectory, to determine the geometrical stability of the protein-ligand complex and are shown in (Figure 5 and Figure 6, respectively) [56]. Out of all the studied ligands, only two ligands showed smooth and stable RMSD curves

with α -glucosidase protein, and only one showed an acceptable RMSD value with α -amylase. The ligands 1 and 2 showed smooth RMSD curves with α -glucosidase along with an equilibrated RMSD of the ligands below 6.5 Å. Compound 1 exhibited higher geometrical stability, with RMSD below 5 Å after equilibration around 60 ns. Despite several spikes in the trajectory in the case of compound 2, the smooth RMSD curve was obtained, and the system remained equilibrated with RMSD ca. 6.5 Å after approximately 75 ns. The smooth and steady nature of the RMSD curves of protein backbones at approximately 2.2 Å indicates the stability of the 3D geometry of protein upon ligand binding.

In the case of α -amylase, compound 1 showed a smooth trajectory with minute peaks with an RMSD value below 6 Å. After about 25 ns, the system attained equilibrium and remained almost the same up to 200 ns. The RMSD of the backbone remained fairly stable below 2 Å, indicating the stability of the α -amylase structure. Since compound 1 showed better stability with both α -glucosidase and α -amylase protein, it could be inferred that the molecule is possibly capable of disrupting both receptor molecules [57].

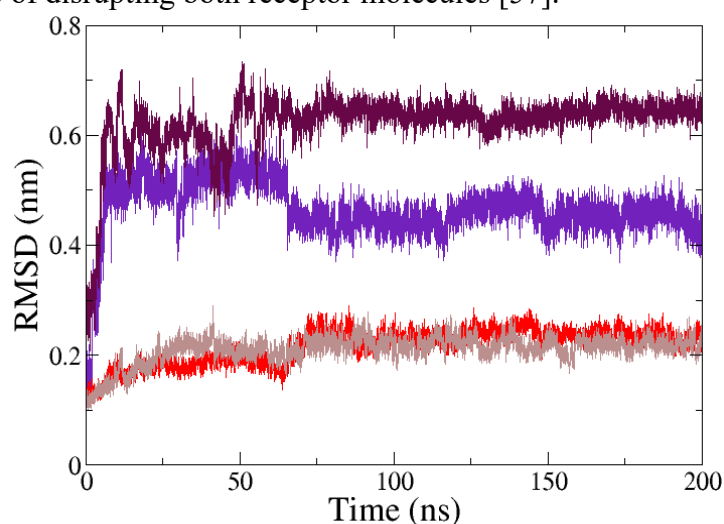


Figure 5. RMSD curves of compound 1 (**indigo**) and 2 (**maroon**) with respect to protein backbone in 1- α -glucosidase complex and 2- α -glucosidase complex, respectively. RMSD curve of protein backbone (**red**) with respect to protein backbone in 1- α -glucosidase complex; RMSD curve of protein backbone (**brown**) with respect to protein backbone in 2- α -glucosidase complex.

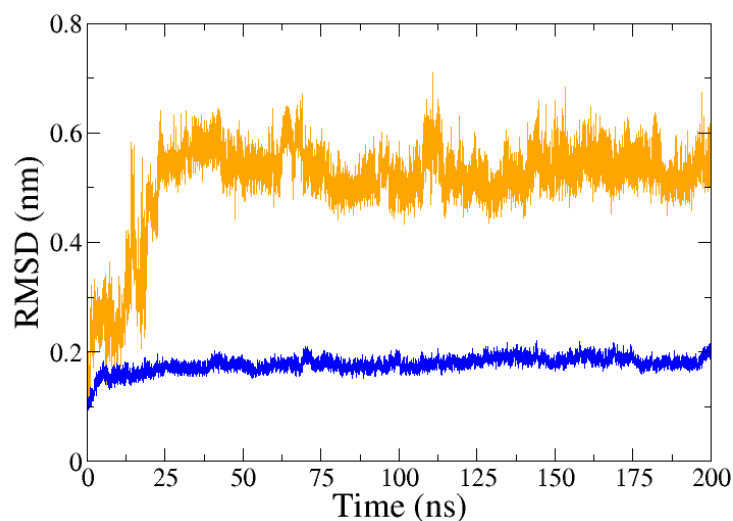


Figure 6. RMSD curve of compound 1 (**orange**) with respect to protein backbone in 1- α -amylase complex; RMSD curve of protein backbone (**blue**) with respect to protein backbone in 1- α -amylase complex.

3.9.2. Root mean square fluctuation (RMSF).

The RMSF value is a quantitative measure employed to assess the fluctuation of amino acid residues at their mean position in the protein upon ligand binding [58]. Higher RMSF values indicate more flexible structural elements like turns and loops, whereas lower RMSF values point to the existence of secondary structures like helices and sheets that are more stable and resist motion [59]. The RMSF plots depict the lower fluctuations of amino acid residues at the catalytic sites of the protein relative to other amino acid residues of the protein, which indicates that no significant conformational changes of the receptor protein structure occurred upon ligand binding.

In the case of the α -glucosidase complex, the highest fluctuation of amino acid residues, i.e., ca. 4.8 Å, was observed between amino acid residues 505 and 545 due to the presence of a highly unstable loop structure at the terminus of the receptor protein (more than 30 Å from the ligand-binding site) as shown in (Figure S2). Whereas in the case of α -amylase, the highest fluctuation of amino acid residues, i.e., ca. 3.4 Å, was observed between the amino acid 240-370 due to highly fluctuating loop structures at distances 16-29 Å from the catalytic site as depicted in (Figure S3). Thus, the fluctuation can be neglected as their motion doesn't affect ligand binding. Moreover, RMSF below approximately 0.5 Å was observed with the catalytic triad of α -amylase: ASP197, GLU233, and ASP300 upon ligand binding.

3.9.3. Radius of gyration (R_g).

The radius of gyration is used to assess the conformation changes of protein during MD simulation, such as the expansion and contraction of receptor molecules upon ligand binding [60]. It measures the degree of separation of each element from the central axis of protein.

In the case of α -glucosidase, a slight variation of about 0.4 Å was observed between the ligands 1 and 2 complexes, as displayed in (Figure S4). The R_g of ligand 1 slightly decreased from 24.6 Å to 24.2 Å, inferring a negligible contraction of protein, whereas the smooth, stable trajectory of 2 indicated no observable receptor shrinking or expansion in response to ligand binding. Similarly, a smooth R_g trajectory with a value of 23.5 Å was observed in α -amylase protein, as shown in (Figure S5). The steady nature of the curve emphasizes the stability in terms of the folding or unfolding of the protein geometry. Both the protein structures were stable with no significant compression and expansion during the 200 ns production run.

3.9.4. Solvent accessible surface area (SASA).

Solvent-accessible surface area (SASA) helps to evaluate the wettable portion of the protein molecule [61]. The SASA for ligands 1 and 2- α -glucosidase complexes were approximately 245 nm² and 235 nm² as presented in (Figure S6). Similarly, SASA of 205 nm² was observed with 1-amylase complex as shown in (Figure S7). These values and the smooth nature of the curve imply that the protein's hydrophobic portion remains unexposed to the solvent during ligand binding, maintaining its geometric integrity, as reported by Zhang and Lazim [62]. The smooth trajectory for 200 ns for both ligands indicated no variation in protein morphology and solvent-accessible region of the protein upon ligand binding.

3.9.5. Hydrogen bond count.

The number of hydrogen bonds governs the geometrical stability of the system since it is the strongest type of non-covalent interaction [63]. The larger the number of hydrogen bonds and the shorter the distance formed between the ligand and protein, the greater the stability of the complex, as reflected in the RMSD profile of ligands as illustrated in (Figure 5 and Figure 6). In both the adducts, the ligand formed a higher number of hydrogen bonds, reaching up to 7. In the case of α -glucosidase, both the ligands 1 and 2 formed multiple hydrogen bonds with the receptor during 200 ns, supporting the localization of the ligand at the active site. Complex 1 exhibited more hydrogen bonds, reaching up to 7 at certain instances and consistently maintaining up to 4 after approximately 70 ns, as shown in (Figure S8). In contrast, complex 2 showed a maximum of 5 and constantly 3 hydrogen bonds after 80 ns between the ligand and the receptor, as displayed in (Figure S9). The presence of a higher number of hydrogen bonds in complex 1 contributed to the formation of a more stable complex, as reflected in comparatively lower RMSD values of 5 Å, as shown in (Figure 5). In the 1- α -amylase complex, up to 7 hydrogen bonds were observed at the beginning up to around 15 ns, as shown in (Figure S10). The decrease in the number of hydrogen bonds thereafter could have resulted in a rise in RMSD, as shown in (Figure 6). Later, after the equilibration, with consistent 4 or 5 hydrogen bonds, the RMSD curve remained smooth and stationary up to 200 ns. In this way, the number of hydrogen bonds could be correlated to the RMSD profile of ligands [64].

The stability of the system in terms of the RMSD of the ligand could be correlated with the number of hydrogen bonds formed between the ligand and the receptor molecule. An inversely proportional relationship could be observed between the number of hydrogen bonds and the RMSD of ligands. The consistency of a larger number of hydrogen bonds formed between the ligand and the protein suggested stronger binding at the orthosteric site, which is capable of inhibiting the normal functioning of the protein.

3.9.6. Spontaneity of complex formation reaction.

Binding free energy change (ΔG_{BFE}) helps to evaluate the spontaneity and feasibility of the complex formation [65,66] and is presented in (Table 3). Binding free energy plots of 20 ns or 200 frames were retrieved from the equilibrated portion of the MDS trajectory from the MMPBSA method for all the complexes, as shown in (Figures S11, S12, and S13). Higher negative values of ΔG_{BFE} for both complexes indicated the feasibility of complex formation. The average binding free energy changes of -24.70 ± 7.94 and -34.56 ± 6.11 kcal/mol for the ligands 1 and 2- α -glucosidase complexes, respectively, suggest the spontaneous nature of the reaction and the thermodynamic stability of the system. In the case of the 1- α -amylase complex, a binding free energy change of -14.47 ± 6.19 kcal/mol also indicated the spontaneous nature of the adduct formation reaction. Thermodynamic spontaneity was maintained until the end of the production run.

Table 3. Change in binding free energy (kcal/mol) of complexes with different components for 20 ns from the MMPBSA method.

Complex	ΔE_{VDW}	ΔE_{EEL}	ΔE_{PB}	ΔE_{NPOLAR}	ΔG_{GAS}	ΔG_{SOLV}	ΔG_{BFE}
1- α -glucosidase	-55.50±	-43.69±	80.32±	-5.83± 0.12	-99.19±	74.49±	-24.70±
	3.24	7.44	8.75		7.04	8.75	7.94
2- α -glucosidase	-58.71±	-28.00±	58.72±	-6.58± 0.25	-86.71±	52.14±	-34.56±
	3.59	5.58	8.84		6.95	8.72	6.11
1- α -amylase	-48.63±	-21.21±	60.74±	-5.37± 0.26	-69.84±	55.37±	-14.47±
	3.56	8.00	8.63		8.20	8.27	6.19

The spontaneity of the forward reaction was indicated by the consistent negative values across frames, suggesting that it constantly remained at negative levels. The largest change in binding free energy of -48 kcal/mol at 195 ns was observed in the 2- α -glucosidase complex, indicating the most stable point thermodynamically achieved by any ligand. Average negative ΔG_{BFE} (red curve) indicated that the overall reaction was spontaneous in nature, whereas frame-by-frame evaluation of ΔG_{BFE} implied the sustained spontaneity and feasibility even for the last 20 ns of the MDS trajectory as depicted in (Figure 5 and Figure 6).

The stable trajectories (RMSD, RMSF, SASA, and Rg) and negative binding free energies indicated geometrical and thermodynamic stability of the protein-ligand systems, respectively. The binding affinity, MDS trajectory, and binding free energy collectively support the notion that compound 1 can inhibit both receptor proteins (α -glucosidase and α -amylase) by spontaneously binding at the catalytic site with greater stability. On the other hand, the results suggest that compound 2 could also perform as a potential inhibitor of α -glucosidase.

4. Conclusions

The possibility of diabetes management by the plant *Rubia manjith* Roxb. was investigated by experimental methods, and the chemical compounds present in it were tested by computational tools. The *in vitro* results showed the inhibition of α -amylase and α -glucosidase enzymes. The molecular docking calculations for the molecular-level understanding of the ligand binding with the receptor protein, followed by molecular dynamics simulations of the adduct for stability assessment, were carried out. The binding affinities of 15 phytochemicals against both enzymes revealed that the two compounds (1 and 2) were better than the native ligand. Compound 1 formed a geometrically and thermodynamically stable adduct due to the presence of strong interactions with the active site amino acid residues in both enzymes. Compound 2 exhibited strong binding with the latter enzyme and acceptable stability of its adduct. Validation of the preliminary findings, along with the drug-likeness and safety assessments, could be carried out further by additional *in silico*, *in vitro*, and *in vivo* trials in order to develop effective drugs from plant-based resources.

Author Contributions

Conceptualization, B.P.M., R,L.S.S., and J.A.S.; methodology, S.K., S.D., B.G., K.S.; software, P.N., and M.P.; validation, S.B., B.M., T.S., P.N., and M.P.; formal analysis, J.A.S., B.P.M., and R,L.S.S.; investigation, S.K., S.D., B.G., K.S., P.N., M.P., S.B., B.M., and T.S.; resources, R,L.S.S.; writing—original draft preparation, S.K., P.N., and M.P.; writing—review and editing, J.A.S., B.P.M., and R.L.S.S.; supervision, J.A.S., B.P.M., and R,L.S.S.; project administration, B.P.M.; funding acquisition, R,L.S.S.. All authors have read and agreed to the published version of the manuscript.

Institutional Review Board Statement

Not applicable.

Informed Consent Statement

Not applicable.

Data Availability Statement

Data supporting the findings of this study are available upon reasonable request from the corresponding author.

Funding

This research received no external funding.

Acknowledgments

We appreciate the support provided by Kathmandu Valley College, Kalanki, Kathmandu, for carrying out computational study.

Conflicts of Interest

The authors declare no conflict of interest.

References

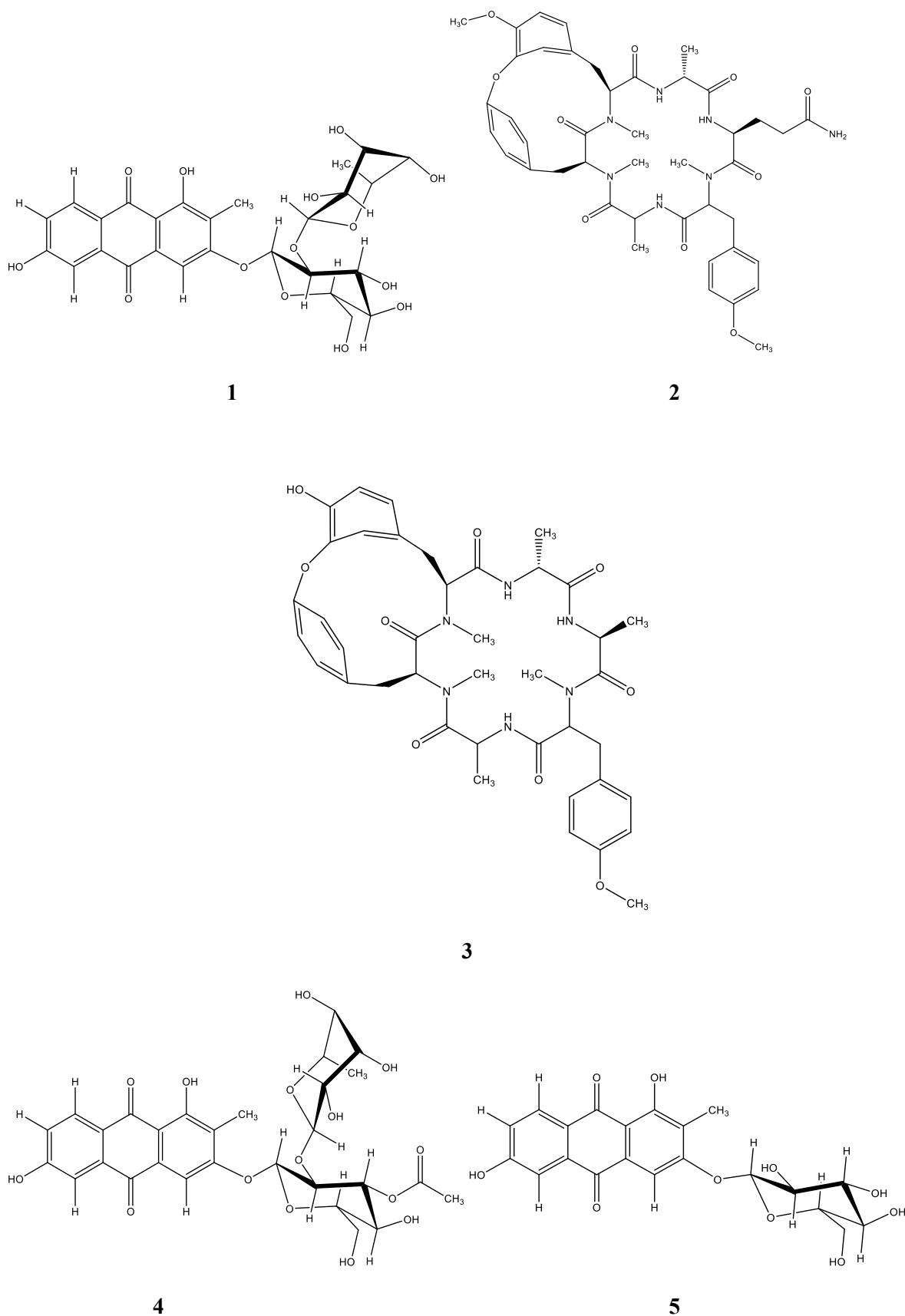
1. Introduction. In IARC MONOGRAPHS ON THE EVALUATION OF CARCINOGENIC RISKS TO HUMANS. IARC Press: Lyon, France, **2002**; Volume 82, pp. 43–68.
2. Okigbo, R.N.; Eme, U.E.; Ogbogu S. Biodiversity and conservation of medicinal and aromatic plants in Africa. *Biotechnol. Mol. Biol. Rev.* **2008**, *3*, 127–134.
3. Cowan, M.M. Plant products as antimicrobial agents. *Clin. Microbiol. Rev.* **1999**, *12*, 564–582, <https://doi.org/10.1128/CMR.12.4.564>.
4. Vaou, N.; Stavropoulou, E.; Voidarou, C.; Tsigalou, C.; Bezirtzoglou, E. Towards advances in medicinal plant antimicrobial activity: A review study on challenges and future perspectives. *Microorganisms* **2021**, *9*, 2041, <https://doi.org/10.3390/microorganisms9102041>.
5. Pradhan, D.K.; Ulak, S.; Charmakar, S.; Kunwar, R.M.; Bussmann, R.W.; Paniagua-Zambrana, N.Y. *Rubia manjith Roxb. ex Fleming Rubia tinctorium L. Rubiaceae*. In Ethnobotany of the Himalayas, Kunwar, R.M., Sher, H., Bussmann, R.W., Eds.; Springer International Publishing: Cham, **2021**; pp. 1709–1716., https://doi.org/10.1007/978-3-030-57408-6_207.
6. Kumari, I.; Kaurav, H.; Choudhary, G. *Rubia cordifolia* (Manjishtha): A review based upon its ayurvedic and medicinal uses. *Himal. J. Heal. Sci.* **2021**, *6*, 17–28, <https://doi.org/10.22270/hjhs.v6i2.96>.
7. Huang, S.; Zou, X. Advances and challenges in protein-ligand docking. *Int. J. Mol. Sci.* **2010**, *11*, 3016–3034, <https://doi.org/10.3390/ijms11083016>.
8. Neupane, P.; Dhital, S.; Parajuli, N.; Shrestha, T.; Bharati, S.; Maharjan, B.; Adhikari Subin, J.; Shrestha, R.L.S. Exploration of anti-diabetic potential of *Rubus ellipticus* smith through molecular docking, molecular dynamics simulation, and MMPBSA calculation. *J. Nepal Phys. Soc.* **2023**, *9*, 95–105, <https://doi.org/10.3126/jnphysoc.v9i2.62410>.

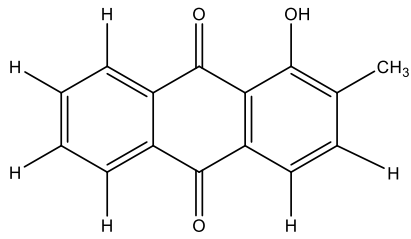
9. Kaur, N.; Kumar, V.; Nayak, S.K.; Wadhwa, P.; Kaur, P.; Sahu, S.K. Alpha-amylase as molecular target for treatment of diabetes mellitus: A comprehensive review. *Chem. Biol. Drug Des.* **2021**, *98*, 539–560, <https://doi.org/10.1111/cbdd.13909>.
10. Shrestha, R.L.S.; Panta, R.; Maharjan, B.; Shrestha, T.; Bharati, S.; Dhital, S.; Neupane, P.; Parajuli, N.; Marasini, B.P.; Adhikari Subin, J. Molecular docking and ADMET prediction of compounds from Piper longum L. Detected by GC-MS analysis in diabetes management. *Mor. J. Chem.* **2024**, *12*, 776–798, <https://doi.org/10.48317/IMIST.PRSM/morjchem-v12i2.46845>.
11. Toniolo, A.; Cassani, G.; Puggioni, A.; Rossi, A.; Colombo, A.; Onodera, T.; Ferrannini, E. The diabetes pandemic and associated infections: Suggestions for clinical microbiology. *Rev. Med. Microbiol.* **2019**, *30*, 1–17, <https://doi.org/10.1097/MRM.000000000000155>.
12. Kumar, V.; Prakash, O.; Kumar, S.; Narwal, S. α -glucosidase inhibitors from plants: A natural approach to treat diabetes. *Pharmacogn. Rev.* **2011**, *5*, 19, <https://doi.org/10.4103/0973-7847.79096>.
13. Kumar, A.; Singh, S.K.; Singh, V.K.; Kant, C.; Singh, A.K.; Tripathi, V.; Singh, K.; Sharma, V.K.; Singh, J. An insight into the molecular docking interactions of plant secondary metabolites with virulent factors causing common human diseases. *South African J. Bot.* **2022**, *149*, 1008–1016, <https://doi.org/10.1016/j.sajb.2021.11.010>.
14. Ainsworth, E.A.; Gillespie, K.M. Estimation of total phenolic content and other oxidation substrates in plant tissues using Folin–Ciocalteu reagent. *Nat. Protoc.* **2007**, *2*, 875–877, <https://doi.org/10.1038/nprot.2007.102>.
15. Chang, C.; Yang, M.; Wen, H.; Chern, J. Estimation of total flavonoid content in propolis by two complementary colometric methods. *J. Food Drug Anal.* **2020**, *10*, <https://doi.org/10.38212/2224-6614.2748>.
16. Sabudak, T.; Demirkiran, O.; Ozturk, M.; Topcu, G. Phenolic compounds from *Trifolium echinatum* Bieb. and investigation of their tyrosinase inhibitory and antioxidant activities. *Phytochem.* **2013**, *96*, 305–311, <https://doi.org/10.1016/j.phytochem.2013.08.014>.
17. Subedi, A.; Amatya, M.P.; Shrestha, T.M.; Mishra, S.K.; Pokhrel, B.M. Antioxidant and antibacterial activity of methanolic extract of *Machilus Odoratissima*. *Kathmandu Univ. J. Sci. Eng. Technol.* **1970**, *8*, 73–80, <https://doi.org/10.3126/kuset.v8i1.6045>.
18. Khadayat, K.; Marasini, B.P.; Gautam, H.; Ghaju, S.; Parajuli, N. Evaluation of the alpha-amylase inhibitory activity of Nepalese medicinal plants used in the treatment of diabetes mellitus. *Clin. Phytosci.* **2020**, *6*, 34, <https://doi.org/10.1186/s40816-020-00179-8>.
19. Fouotsa, H.; Lannang, A.M.; Mbazoa, C.D.; Rasheed, S.; Marasini, B.P.; Ali, Z.; Devkota, K.P.; Kengfack, A.E.; Shaheen, F.; Choudhary, M.I.; Sewald, N. Xanthones inhibitors of α -glucosidase and glycation from *Garcinia nobilis*. *Phytochem. Lett.* **2012**, *5*, 236–239, <https://doi.org/10.1016/j.phytol.2012.01.002>.
20. Balachandran, P.; Ibrahim, M.A.; Zhang, J.; Wang, M.; Pasco, D.S.; Muhammad, I. Crosstalk of cancer signaling pathways by cyclic hexapeptides and anthraquinones from *Rubia cordifolia*. *Molecules* **2021**, *26*, 735, <https://doi.org/10.3390/molecules26030735>.
21. Chen, Y.; Chen, P.; Bao, B.; Shan, M.; Zhang, K.; Cheng, F.; Cao, Y.; Zhang, L.; Ding, A. Anti-thrombotic and pro-angiogenic effects of *Rubia cordifolia* extract in zebrafish. *J. Ethnopharmacol.* **2018**, *219*, 152–160, <https://doi.org/10.1016/j.jep.2017.11.005>.
22. Itokawa, H.; Takeya, K.; Hitotsuyangi, Y.; Morita, H. Antitumor compounds isolated from higher plants. *Yakugaku Zasshi.* **1999**, *119*, 529–583, https://doi.org/10.1248/yakushi1947.119.8_529.
23. Wen, M.; Chen, Q.; Chen, W.; Yang, J.; Zhou, X.; Zhang, C.; Wu, A.; Lai, J.; Chen, J.; Mei, Q.; Yang, S.; Lan, C.; Wu, J.; Huang, F.; Wang, L. A comprehensive review of *Rubia cordifolia* L.: Traditional uses, phytochemistry, pharmacological activities, and clinical applications. *Front. Pharmacol.* **2022**, *13*, 965390, <https://doi.org/10.3389/fphar.2022.965390>.
24. Zeng, W.; Shen, C.; Mo, S.; Ni, C.; Lin, Y.; Fang, Y.; Yang, H.; Luo, G.; Xiao, L.; Zhan, R.; Yan, P. The effective treatment of purpurin on inflammation and adjuvant-induced arthritis. *Molecules.* **2023**, *28*, 366, <https://doi.org/10.3390/molecules28010366>.
25. Zhao, S.M.; Kuang, B.; Fan, J.T.; Yan, H.; Xu, W.Y.; Tan, N.H. Antitumor cyclic hexapeptides from *Rubia* plants: History, chemistry, and mechanism (2005–2011). *Chimia* **2011**, *65*, 952, <https://doi.org/10.2533/chimia.2011.952>.
26. Li, Z.; Wan, H.; Shi, Y.; Ouyang, P. Personal experience with four kinds of chemical structure drawing software: Review on ChemDraw, ChemWindow, ISIS/Draw, and ChemSketch. *J. Chem. Inf. Comput. Sci.* **2004**, *44*, 1886–1890, <https://doi.org/10.1021/ci049794h>.

27. López, R. Capillary surfaces with free boundary in a wedge. *Adv. Math.* **2014**, *262*, 476–483, <https://doi.org/10.1016/j.aim.2014.05.019>.
28. Trott, O.; Olson, A.J. AutoDock Vina: Improving the speed and accuracy of docking with a new scoring function, efficient optimization, and multithreading. *J. Comput. Chem.* **2010**, *31*, 455–461, <https://doi.org/10.1002/jcc.21334>.
29. Berman, H.M. The Protein Data Bank. *Nucleic Acids Res.* **2000**, *28*, 235–242, <https://doi.org/10.1093/nar/28.1.235>.
30. Waterhouse, A.; Bertoni, M.; Bienert, S.; Studer, G.; Tauriello, G.; Gumienny, R.; Heer, F.T.; de Beer, T.A.P.; Rempfer, C.; Bordoli, L.; Lepore, R.; Schwede, T. SWISS-MODEL: Homology modelling of protein structures and complexes. *Nucleic Acids Res.* **2018**, *46*, W296–W303, <https://doi.org/10.1093/nar/gky427>.
31. Yuan, S.; Chan, H.C.S.; Hu, Z. Using <sc>PyMOL</sc> as a platform for computational drug design. *WIREs Comput. Mol. Sci.* **2017**, *7*, e1298, <https://doi.org/10.1002/wcms.1298>.
32. Jain, A.N. Surflex: Fully automatic flexible molecular docking using a molecular similarity-based search engine. *J. Med. Chem.* **2003**, *46*, 499–511, <https://doi.org/10.1021/jm020406h>.
33. Li, X.; Li, Y.; Cheng, T.; Liu, Z.; Wang, R. Evaluation of the performance of four molecular docking programs on a diverse set of protein-ligand complexes. *J. Comput. Chem.* **2010**, *31*, 2109–2125, <https://doi.org/10.1002/jcc.21498>.
34. Ramírez, D.; Caballero, J. Is it reliable to take the molecular docking top scoring position as the best solution without considering available structural data? *Molecules* **2018**, *23*, 1038, <https://doi.org/10.3390/molecules23051038>.
35. Baroroh, S.Si.; Muscifa, Z.S.; Destiarani, W.; Rohmatullah, F.G.; Yusuf, M. Molecular interaction analysis and visualization of protein-ligand docking using Biovia Discovery Studio Visualizer. *Indones J. Comput. Biol.* **2023**, *2*, 22, <https://doi.org/10.24198/ijcb.v2i1.46322>.
36. Abraham, M.J.; Murtola, T.; Schulz, R.; Páll, S.; Smith, J.C.; Hess, B.; Lindahl, E. GROMACS: High performance molecular simulations through multi-level parallelism from laptops to supercomputers. *SoftwareX* **2015**, *1–2*, 19–25, <https://doi.org/10.1016/j.softx.2015.06.001>.
37. Foloppe, N.; MacKerell, Jr. All-atom empirical force field for nucleic acids: I. parameter optimization based on small molecule and condensed phase macromolecular target data. *J. Comput. Chem.* **2000**, *21*, 86–104, [https://doi.org/10.1002/\(SICI\)1096-987X\(20000130\)21:2<86::AID-JCC2>3.0.CO;2-G](https://doi.org/10.1002/(SICI)1096-987X(20000130)21:2<86::AID-JCC2>3.0.CO;2-G).
38. Zoete, V.; Cuendet, M.A.; Grosdidier, A.; Michielin, O. SwissParam: A fast force field generation tool for small organic molecules. *J. Comput. Chem.* **2011**, *32*, 2359–2368, <https://doi.org/10.1002/jcc.21816>.
39. Neupane, P.; Adhikari Subin, J.; Adhikari, R. Assessment of iridoids and their similar structures as antineoplastic drugs by in silico approach. *Journal of Biomolecular Structure and Dynamics* **2024**, 1–16, <https://doi.org/10.1080/07391102.2024.2314262>.
40. Sharma, B.P.; Adhikari, S.J.; Marasini, B.P.; Adhikari, R.; Pandey, S.K.; Sharma, M.L. Triazole based Schiff bases and their oxovanadium(IV) complexes: Synthesis, characterization, antibacterial assay, and computational assessments. *Heliyon* **2023**, *9*, e15239, <https://doi.org/10.1016/j.heliyon.2023.e15239>.
41. Valdés-Tresanco, M.S.; Valdés-Tresanco, M.E.; Valiente, P.A.; Moreno, E. gmx_MMPBSA: A new tool to perform end-state free energy calculations with GROMACS. *J. Chem. Theory Comput.* **2021**, *17*, 6281–6291, <https://doi.org/10.1021/acs.jctc.1c00645>.
42. Dong, L.; Qu, X.; Zhao, Y.; Wang, B. Prediction of binding free energy of protein-ligand complexes with a hybrid molecular mechanics/generalized born surface area and machine learning method. *ACS Omega* **2021**, *6*, 32938–32947, <https://doi.org/10.1021/acsomega.1c04996>.
43. Chandrashekar, B.; Prabhakara, S.; Mohan, T.; Shabeer, D.; Bhandare, B.; Nalini, M.; Sharmila, P.; Meghana, D.; Reddy, B.; Hanumantha Rao, H.; Sahajananda, H.; Anbazhagan, K. Characterization of *Rubia cordifolia* L. root extract and its evaluation of cardioprotective effect in Wistar rat model. *Indian J. Pharmacol.* **2018**, *50*, 12, https://doi.org/10.4103/ijp.IJP_418_17.
44. Patil, R.; Gadakh, R.; Gound, H.; Kasture, S. Antioxidant and anticholinergic activity of *Rubia Cordifolia*. *Pharmacologyonline* **2011**, *2*, 272–278.
45. Siril, E.A. Traditional and modern use of Indian madder (*Rubia cordifolia* L.): An overview. *Int. J. Pharm. Sci. Res.* **2014**, *25*, 154–164.
46. Deoda, R.S.; Kumar, D.; Kadam, P.V.; Yadav, K.N.; Bhujbal, S.S.; Patil, M.J. Pharmacognostic and biological studies of the roots of *Rubia Cordifolia* linn. (Rubiaceae). *Int. J. Drug Dev. Res.* **2011**, *3*, 148–158.

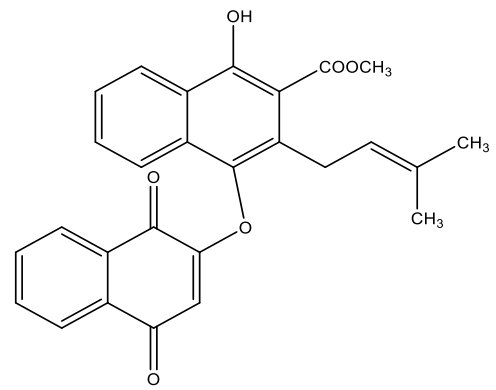
47. Srabana, M.; Kshitij, S. Ethano-botanical studies on *Rubia cordifolia* linn. *Int. J. Recent Sci. Res.* **2017**, *8*, 22264–22267, <https://doi.org/10.24327/IJRSR>.
48. Manach, C.; Scalbert, A.; Morand, C.; Rémésy, C.; Jiménez, L. Polyphenols: Food sources and bioavailability. *Am. J. Clin. Nutr.* **2004**, *79*, 727–747, <https://doi.org/10.1093/ajcn/79.5.727>.
49. Kunwar, R.M.; Uprety, Y.; Burlakoti, C.; Chowdhary, C.L.; Bussmann, R.W. Indigenous use and ethnopharmacology of medicinal plants in far-west Nepal. *Ethnobot. Res. App.* **2009**, *7*, 5–28.
50. Kang, W.; Zhang, L.; Song, Y. Alpha-glucosidase inhibitors from *Rubia cordifolia*. *China J. Chinese Mater. medica.* **2009**, *34*, 1104–1107.
51. Kitchen, D.B.; Decornez, H.; Furr, J.R.; Bajorath, J. Docking and scoring in virtual screening for drug discovery: Methods and applications. *Nat. Rev. Drug Discov.* **2004**, *3*, 935–949, <https://doi.org/10.1038/nrd1549>.
52. Erickson, J.A.; Jalaie, M.; Robertson, D.H.; Lewis, R.A.; Vieth, M. Lessons in molecular recognition: The effects of ligand and protein flexibility on molecular docking accuracy. *J. Med. Chem.* **2004**, *47*, 45–55, <https://doi.org/10.1021/jm030209y>.
53. Pantsar, T.; Poso, A. Binding affinity via docking: Fact and fiction. *Molecules.* **2018**, *23*, 1899, <https://doi.org/10.3390/molecules23081899>.
54. Hanwell, M.D.; Curtis, D.E.; Lonie, D.C.; Vandermeersch, T.; Zurek, E.; Hutchison, G.R. Avogadro: An advanced semantic chemical editor, visualization, and analysis platform. *J. Cheminform.* **2012**, *4*, 17, <https://doi.org/10.1186/1758-2946-4-17>.
55. Du, X.; Li, Y.; Xia, Y.-L.; Ai, S.-M.; Liang, J.; Sang, P.; Ji, X.-L.; Liu, S.-Q. Insights into protein-ligand interactions: Mechanisms, models, and methods. *Int. J. Mol. Sci.* **2016**, *17*, 144, <https://doi.org/10.3390/ijms17020144>.
56. Adcock, S.A.; McCammon, J.A. Molecular dynamics: Survey of methods for simulating the activity of proteins. *Chem. Rev.* **2006**, *106*, 1589–1615, <https://doi.org/10.1021/cr040426m>.
57. Salo-ahen, O.M.H.; Alanko, I.; Bhadane, R.; Bonvin, A.M.J.J.; Honorato, R.V.; Hossain, S.; Juffer, A.H.; Kabedev, A.; Lahtela-kakkonen, M.; Larsen, A.S.; Lescrinier, E.; Marimuthu, P. Molecular dynamics simulations in drug discovery and pharmaceutical development. *Processes* **2021**, *9*, 71, <https://doi.org/10.3390/pr9010071>.
58. Martínez, L. Automatic identification of mobile and rigid substructures in molecular dynamics simulations and fractional structural fluctuation analysis. *PLoS ONE* **2015**, *10*, 1–10, <https://doi.org/10.1371/journal.pone.0119264>.
59. Sharma, P.; Joshi, T.; Joshi, T.; Chandra, S.; Tamta, S. Molecular dynamics simulation for screening phytochemicals as α -amylase inhibitors from medicinal plants. *J. Biomol. Struct. Dyn.* **2021**, *39*, 6524–6538, <https://doi.org/10.1080/07391102.2020.1801507>.
60. Lobanov, M.I.; Bogatyreva, N.S.; Galzitskaia, O.V. Radius of gyration is indicator of compactness of protein structure. *Mol. Biol. (Mosk).* **2008**, *42*, 701–706.
61. Durham, E.; Dorr, B.; Woetzel, N.; Staritzbichler, R.; Meiler, J. Solvent accessible surface area approximations for rapid and accurate protein structure prediction. *J. Mol. Model.* **2009**, *15*, 1093–1108, <https://doi.org/10.1007/s00894-009-0454-9>.
62. Zhang, D.; Lazim, R. Application of conventional molecular dynamics simulation in evaluating the stability of apomyoglobin in urea solution. *Sci. Rep.* **2017**, *7*, 44651, <https://doi.org/10.1038/srep44651>.
63. Chikalov, I.; Yao, P.; Moshkov, M.; Latombe, J.C. Learning probabilistic models of hydrogen bond stability from molecular dynamics simulation trajectories. *BMC Bioinformatics.* **2011**, *12*, S34, <https://doi.org/10.1186/1471-2105-12-S1-S34>.
64. Kony, D.B.; Hünenberger, P.H.; Gunsteren, W.F. Molecular dynamics simulations of the native and partially folded states of ubiquitin: Influence of methanol cosolvent, pH, and temperature on the protein structure and dynamics. *Protein Sci.* **2007**, *16*, 1101–1118, <https://doi.org/10.1110/ps.062323407>.
65. Cournia, Z.; Allen, B.; Sherman, W. Relative binding free energy calculations in drug discovery: Recent advances and practical considerations. *J. Chem. Inf. Model.* **2017**, *57*, 2911–2937, <https://doi.org/10.1021/acs.jcim.7b00564>.
66. Perozzo, R.; Folkers, G.; Scapozza, L. Thermodynamics of protein–ligand interactions: History, presence, and future aspects. *J. Recept. Signal Transduct.* **2004**, *24*, 1–52, <https://doi.org/10.1081/RRS-120037896>.

Supplementary Materials

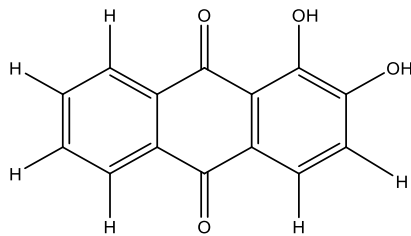




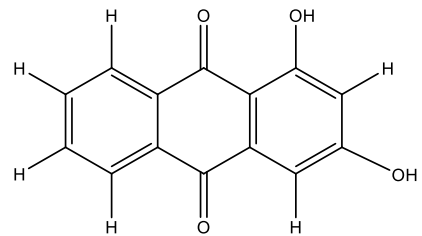
6



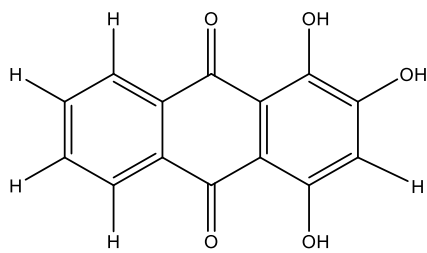
7



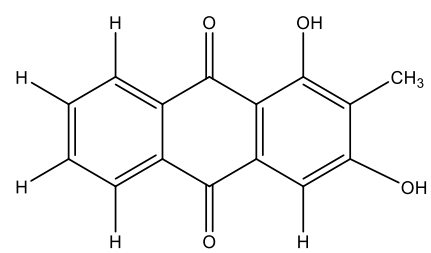
8



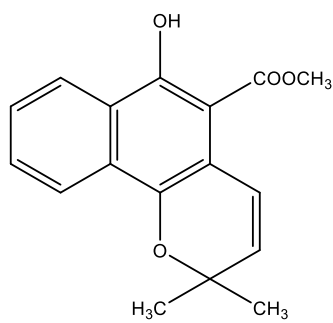
9



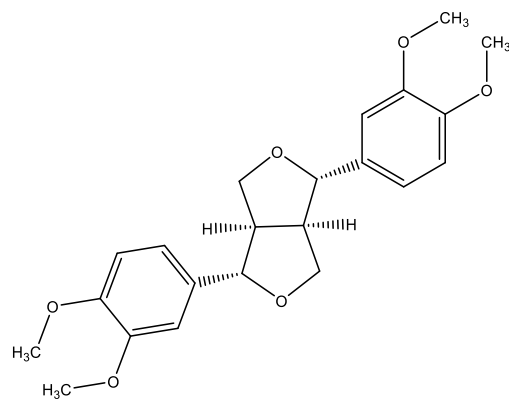
10



11



12



13

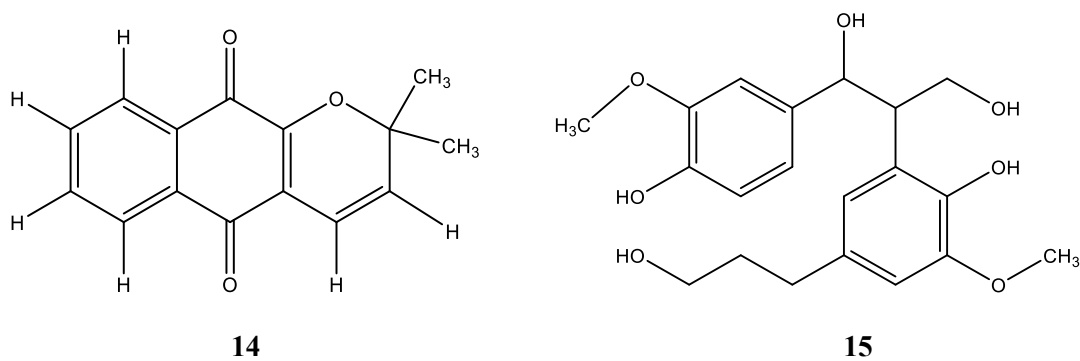


Figure S1. Structure of 15 ligands

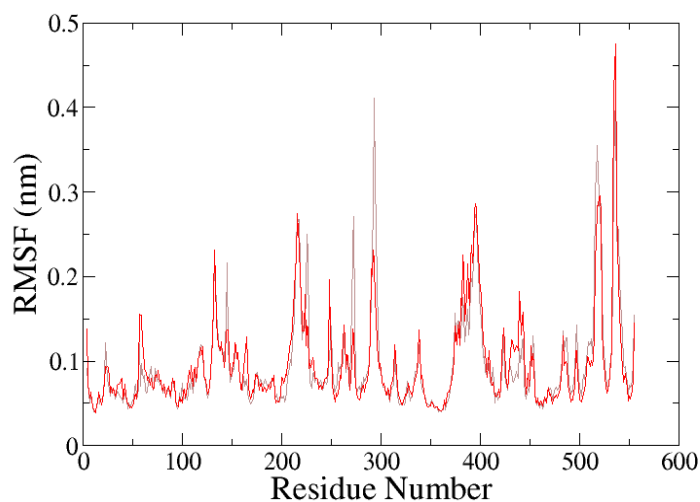


Figure S2. Root mean square fluctuation of α -carbon atoms of α -glucosidase in complex with compound 1 (red) and 2 (brown) calculated from MDS

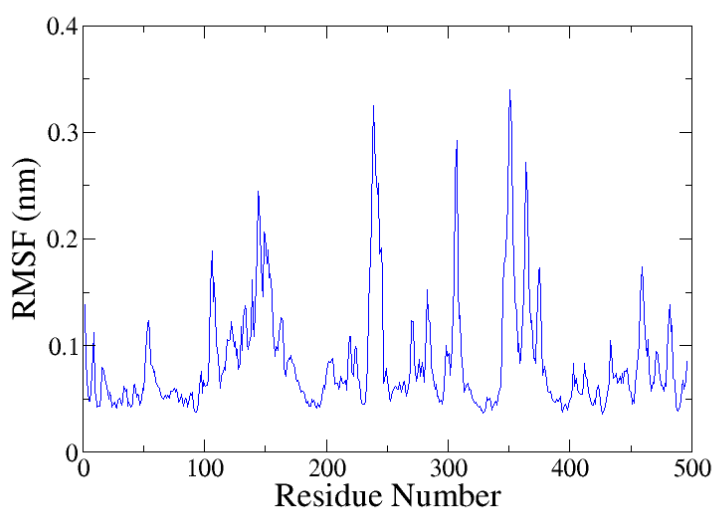


Figure S3. Root mean square fluctuation of α -carbon atoms of α -amylase in complex with compound 1 (blue) calculated from MDS

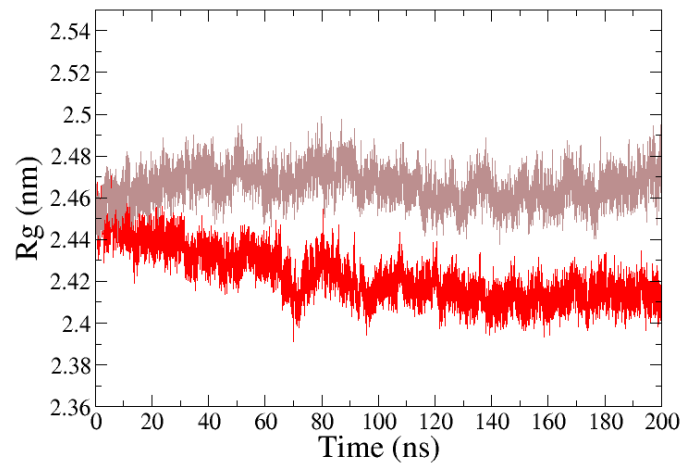


Figure S4. Radius of gyration (R_g) of α -glucosidase structure in complex with compound 1 (red) and 2 (brown)

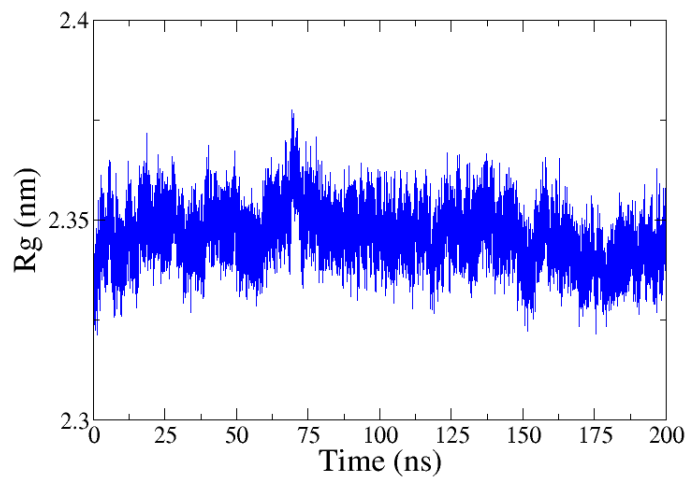


Figure S5. Radius of gyration (R_g) of α -amylase structure in complex with 1 obtained from MDS trajectory

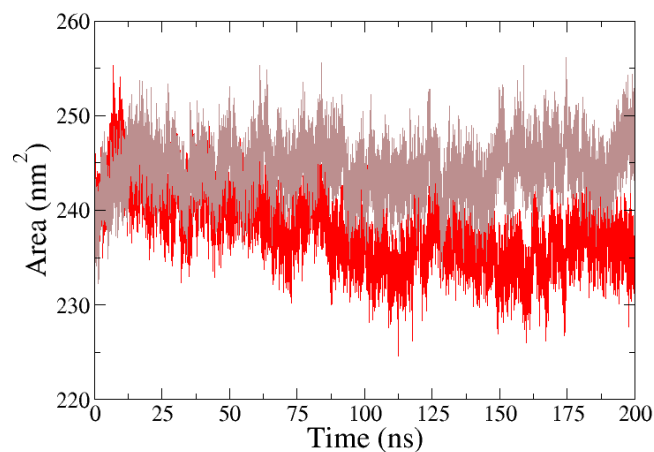


Figure S6. SASA of α -glucosidase in complex with 1 (red) and 2 (brown) calculated from MDS trajectory

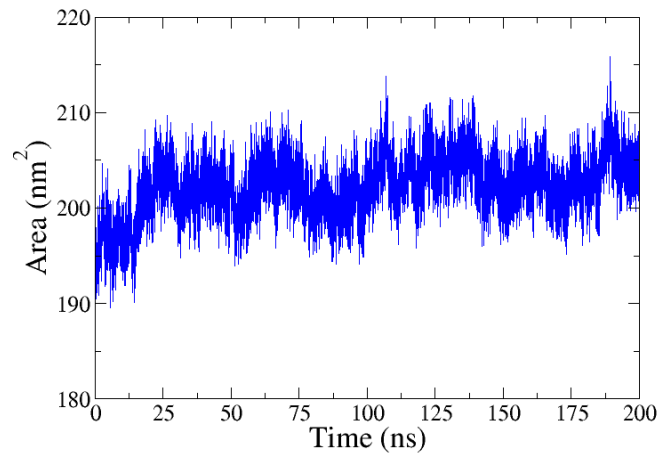


Figure S7. SASA of α -amylase in complex with 1 (blue) extracted from MDS trajectory

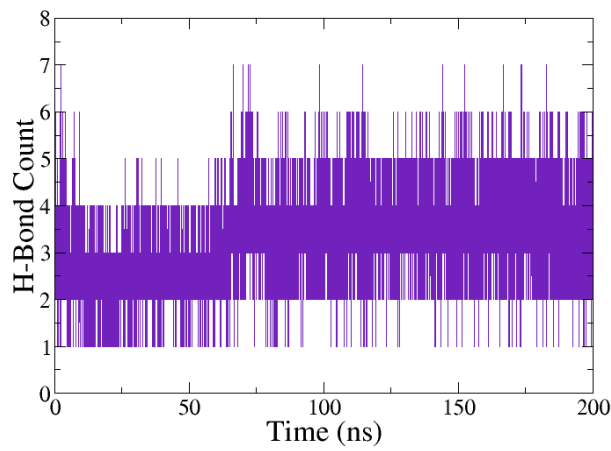


Figure S8. Number of hydrogen bonds between compound 1 and α -glucosidase (indigo) during MDS

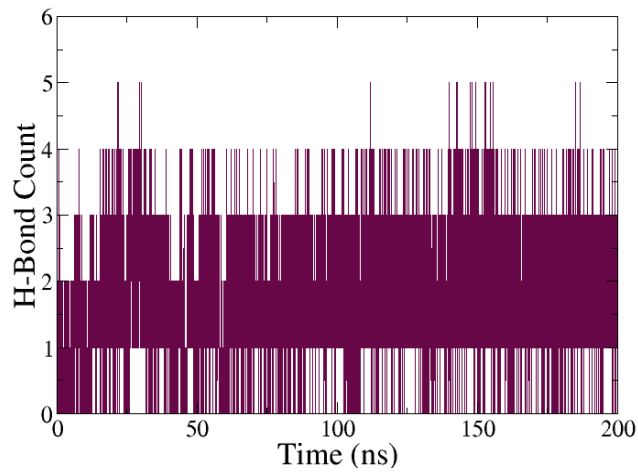


Figure S9. Number of hydrogen bonds between compound 2 and α -glucosidase (maroon) during MDS

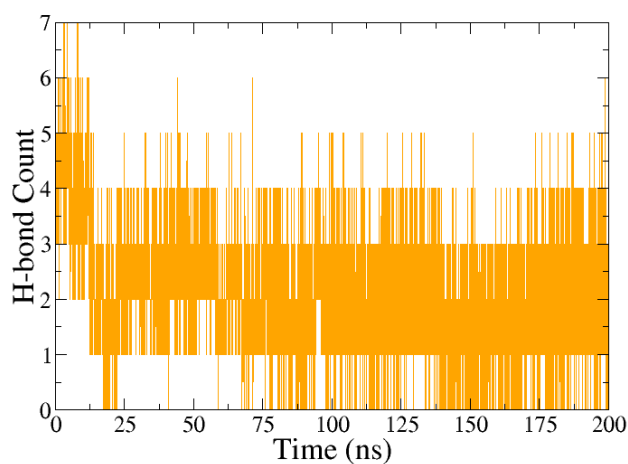


Figure S10. Number of hydrogen bonds between compound 1 and α -amylase (orange) during MDS

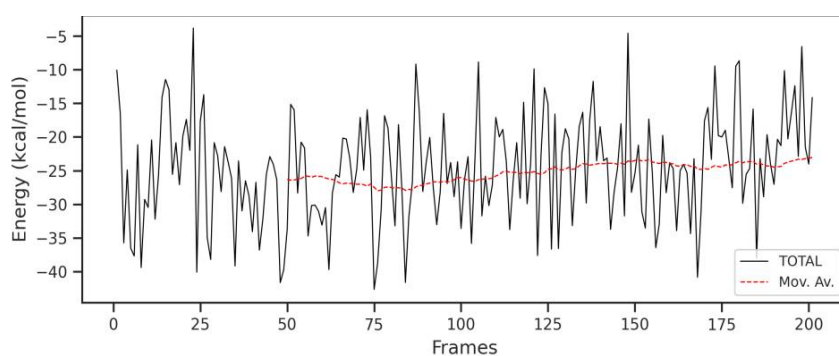


Figure S11. Binding free energy change with time of 1-glucosidase complex

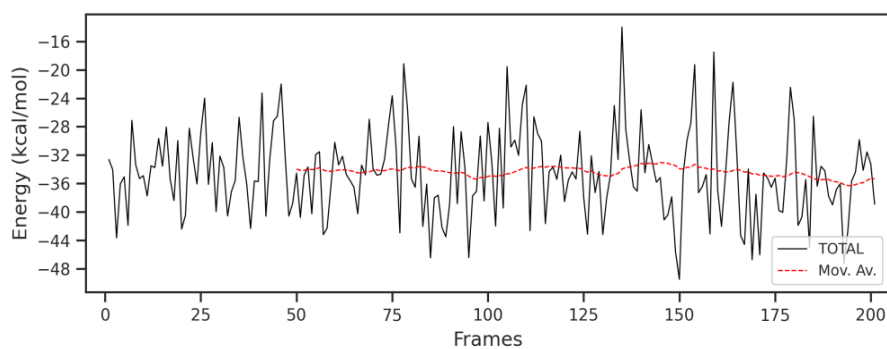


Figure S12. Binding free energy change with time of 1-glucosidase complex

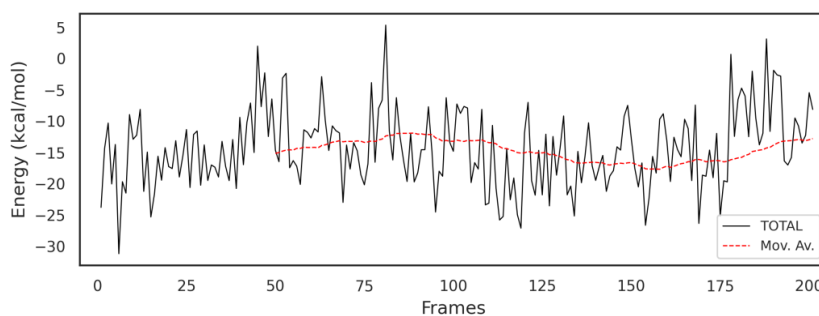


Figure S13. Binding free energy change with time of 1-amylase complex

Table S1. Percentage yield of *R. manjith* extract in different solvent

Solvent name	Yield (%)
Hexane	0.93
Chloroform	1.25
Ethanol	13.08

Table S2. Phytochemical screening of different extracts of *R. manjith*

Plant extracts	Flavo-noid	Alka-loids	Tan-nin	Terpe-noids	Sapo-nin	Phe-nol	Glyco-side	Ster-oids
Chloroform	+	+	+	+	+	+	+	+
Ethanol	+	+	+	+	+	+	+	+

Note: (+) sign indicate the presence and (-) sign indicate absence of phytochemical.

Table S3. Antioxidant activity of plant extracts

Plant extracts	Inhibition (%) at 500µg/mL	IC ₅₀ SEM (µg/mL)
Hexane	43.81	-
Chloroform	87.38	53.07±0.51
Ethanol	52.01	-
Quercetin (standard)	87.01	2.3±0.01

Table S4. Total phenolic content of various extracts of *R. manjith*

TPC± SEM (mg GAE/gm)			
Hexane	Chloroform	Ethanol	Aqueous
2.65±0.01	0.25±0.01	0.10±0.01	-

Table S5. Total flavonoid content of various extracts of *R. manjith*

TFC± SEM (mg QE/gm)			
Hexane	Chloroform	Ethanol	Aqueous
0.03±0.01	0.04±0.01	0.34±0.01	-

TFC values were expressed in mg quercetin equivalent per gram of sample.

Table S6. Alpha-amylase inhibitory activity of various extracts of *R. manjith*

Plant extracts	Enzyme inhibition (%) at 500µg/mL	IC ₅₀ SEM(µg/mL)
Hexane	6.96	-
Chloroform	75.85	113.91±3.62
Ethanol	17	-
Acarbose (standard)	80	6.1±0.04

Table S7. Alpha-glucosidase inhibitory activity of various extracts of *R. manjith*

Plant extracts	Enzyme inhibition (%) at 500µg/mL	IC ₅₀ SEM(µg/mL)
Hexane	41.46	-
Chloroform	72.98	32.89±0.45
Ethanol	25.02	-
Acarbose (standard)	83	387.36±0.05

Table S8. Binding affinities of different ligands with α -glucosidase (PDBID: 5ZCC) and α -amylase (PDBID: 4GQR) protein receptors

Code	Ligands	Binding affinity (kcal/mol)	
		α -glucosidase	α -amylase
1	1,3,6-trihydroxy-2-methylanthraquinone-3-O- α -L-rhamnosyl-(1→2)- β -D-glucoside	-10.0	-9.1
2	Deoxybouvardin RA-XXIII	-9.7	-7.9
3	Deoxybouvardin RA-V	-9.5	-9.7
4	1,3,6-trihydroxy-2-methylanthraquinone-3-O- α -L-rhamnosyl(1→2)- β -D-(3'-O-acetyl)-glucoside	-9.4	-7.2
5	1,3,6-trihydroxy-2-methylanthraquinone-3-O- β -D-glucoside	-8.9	-8.6
6	1-hydroxy-2-methylanthraquinone	-8.6	-7.9
7	Rubioncolin C	-8.5	-8.2

8	Alizarin	-8.2	-7.7
9	Purpuroxanthin	-8.1	-7.6
10	Purpurin	-8.1	-7.8
11	Rubiadin	-8.0	-8.0
12	Mollugin	-8.0	7.0
13	Eudesmin	-7.9	-7.0
14	Dehydro- α -lapachone	-7.9	-7.0
15	2-[2-hydroxy-5-(3-hydroxypropyl)-3-methoxyphenyl]-1-(4-hydroxy-3-methoxyphenyl)propane-1,3-diol	-7.2	-6.5

Publisher's Note & Disclaimer

The statements, opinions, and data presented in this publication are solely those of the individual author(s) and contributor(s) and do not necessarily reflect the views of the publisher and/or the editor(s). The publisher and/or the editor(s) disclaim any responsibility for the accuracy, completeness, or reliability of the content. Neither the publisher nor the editor(s) assume any legal liability for any errors, omissions, or consequences arising from the use of the information presented in this publication. Furthermore, the publisher and/or the editor(s) disclaim any liability for any injury, damage, or loss to persons or property that may result from the use of any ideas, methods, instructions, or products mentioned in the content. Readers are encouraged to independently verify any information before relying on it, and the publisher assumes no responsibility for any consequences arising from the use of materials contained in this publication.